



Shahid Bahonar University of
Kerman



Biomechanism and Bioenergy Research

Online ISSN: 2821-1855
Homepage: <https://bbr.uk.ac.ir>



Iranian Society of Agricultural Machinery
Engineering and Mechanization

Machine Vision Approach Coupled with a Hybrid EHD-Convective Dryer to Model Khalal Slices Drying Process with ANFIS

Aydin Imani¹, Seyed Saeid Mohtasebi² , Alireza Khoshroo³ Mahdi Keramat-Jahromi⁴

¹ Department of Soil Science, Faculty of Agriculture, Urmia University, Urmia, Iran.

² Department of Agricultural Machinery Engineering, Faculty of Agriculture, College of Agriculture and Natural Resources, University of Tehran, Karaj, Iran

³ Department of Agronomy and Plant Breeding, Faculty of Agriculture, Yasouj University, Yasouj, Iran.

⁴ Department of Biosystems Engineering, Faculty of Agriculture, Shiraz University, Shiraz, Iran.

✉ Corresponding author: mohtaseb@ut.ac.ir

ARTICLE INFO

Article type:

Research Article

Article history:

Received 03 February 2025

Received in revised form 07
April 2025

Accepted 31 May 2025

Available Online 30 June 2025

Keywords:

Image processing; EHD;
Khalal; Date palm fruit; Drying;
Moisture ratio; ANFIS.

ABSTRACT

Khalal is a product of date palm fruit before full ripeness and has a higher moisture content than Rutab and fully ripened date fruit. This study deals with monitoring the real-time drying process of Khalal thin slices in a hybrid electro-hydrodynamic (EHD)-convective hot air dryer. The real-time moisture ratio (MR) of Khalal slices was estimated with an intelligent online machine vision system and eliminating the conventional weighing system was investigated. For this purpose, the samples were photographed at specified time intervals during the drying process. An adaptive neuro-fuzzy inference system (ANFIS) was developed to extract real-time models for the drying process. The input features contained different combinations of the temperature of the chamber, air velocity, and drying time along with the L^* , a^* , and b^* coefficients of the image were calculated at different times. The performance of the developed models was evaluated, and the best model was selected. The results revealed that the differential sigmoid membership function with six inputs can provide the best estimation for the moisture ratio (MR) of the product with the coefficient of determination of 0.988 and 0.987 for train and test data, respectively. Finally, it is concluded that the proposed online model can eliminate the need for an embedded weighing system through intelligent control of the EHD-convective dryer and provide a robust real-time prediction of the MR of Khalal thin slices.

Cite this article: Imani, A., Mohtasebi, S. S., Khoshroo, A., & Keramat-Jahromi, M (2025). Machine Vision Approach Coupled with a Hybrid EHD-Convective Dryer to Model Khalal Slices Drying Process with ANFIS. *Biomechanism and Bioenergy Research*, 4(2), 11-25.
<https://doi.org/10.22103/bbr.2025.24768.1116>



© The Author(s).

Publisher: Shahid Bahonar University of Kerman

DOI: <https://doi.org/10.22103/bbr.2025.24768.1116>

INTRODUCTION

Non-thermal electro-hydrodynamic (EHD) dryers are an excellent substitute for conventional thermal dryers with the advantages of drying materials at ambient pressure and temperature as well as better preservation of material properties (Anukiruthika *et al.*, 2021; Martynenko *et al.*, 2017; Martynenko & Kudra, 2016). Although the EHD drying method is not fast compared to the microwave method, it is still a priority in terms of lower energy consumption and high quality of the dried product (Esehaghbeygi *et al.*, 2014; Mirzaei-Baktash *et al.*, 2022). EHD drying method has been studied in various state-of-the-arts (Bashkir *et al.*, 2020; Iranshahi *et al.*, 2022; Paul & Martynenko, 2021; Polat & Izli, 2022a; Polat & Izli 2022b). Two important factors in determining the final quality of a dried product are its color and moisture content (Bora *et al.*, 2018). The color change is an inevitable consequence of a drying process which strongly impacts consumer acceptance (Udomkun *et al.*, 2017). The moisture content of the dried fruit or vegetable depends on the utilized drying method. Excessive drying results in shrinkage of the dried product, deteriorating its final quality (Bora *et al.*, 2018).

Monitoring the quality of the product is of great importance during the drying process. Various studies have mentioned imaging technology as an efficient method to control and monitor product quality (Aghbashlo *et al.*, 2014; Martynenko, 2017). The quality of different products including kernels (Ghaitaranpour *et al.*, 2017), mango (Pu & Sun, 2017), nectarine (Miraei Ashtiani *et al.*, 2018), apples (Aghilinategh *et al.*, 2016; Gao *et al.*, 2017; Nadian *et al.*, 2015), papaya (Udomkun *et al.*, 2017), kiwi (Nadian *et al.*, 2017), fig (Benalia *et al.*, 2016), and Shrimp (Hosseinpour *et al.*, 2013; Hosseinpour *et al.*, 2015) have been studied in various dryers via imaging systems. Several studies have considered the application of offline image processing in EHD dryers for monitoring color change in different fruits, including mushroom slices (Taghian Dinani *et al.*, 2014), thin sheets of banana (Pirnazari *et al.*, 2014), and apple (Martynenko & Zheng, 2016).

Intelligent control of the drying process can be achieved by introducing models that relate the product quality to the image characteristics. Some studies have been conducted to model the color properties of different products (Hosseinpour *et al.*, 2013; Martynenko & Zheng, 2016).

Samples of the peel from pomelo fruit (*Citrus maxima*) were dried by freeze-drying (FD), forced convection (FCD), and microwave drying in two distinct thicknesses (Kırbaş *et al.*, 2019). Experimental results revealed that thin samples dried in a shorter period in all drying methods. Then two models were developed with ANN and machine learning based on the experimental data for the mass-dependent parameters like moisture ratio and the drying time prediction. Microwave vacuum drying of dragon fruit slices with back-propagation and feed-forward ANN was proposed (Raj & Dash, 2020). Sixty experiments were conducted and analysed for independent variables for genetic algorithm optimization. Prediction according to the ANN-GA model had an excellent agreement and slight deviation with experimental data (Shafaei *et al.*, 2016), wheat's hydration characteristics (moisture ratio, moisture content, and hydration rate) were also examined with the help of ANFIS.

This paper addresses the monitoring of the drying process of Shahani variety of date fruits in EHD dryers. A serious challenge of EHD dryers is the disturbance occurring in electrical systems due to the electric field and their high voltage. This makes the conventional weighing systems used in EHD dryers subject to noise. Thus, online monitoring of the drying process in EHD dryers by weighing the dried fruit to estimate its moisture content is very complicated. The main novelty of this study is addressing the problem of online monitoring of the EHD dryers by replacing the conventional weighing system with an intelligent online machine vision-based procedure. To this end, a system consisting of two units, i.e., image acquisition and processing unit, is developed. The acquisition unit captures images of the fruits in various stages of the drying process. The captured images are then

simultaneously processed in the processing unit via a machine vision-based model. In this model, the images are first transformed into L*a*b* color system. Then, an Adaptive Neuro-Fuzzy Inference System (ANFIS) model is used to predict the moisture content of the fruits using different sets of features. Finally, the accuracy of ANFIS model is compared with conventional non-linear regression models to select the best model for predicting moisture ratio of date fruit.

MATERIALS AND METHODS

In this study, a machine vision system is used to monitor the drying process of the collected date fruit samples. The developed system consists of two main units: the image processing unit and the processing unit. The image processing unit includes a Microsoft LifeCam Studio (Q2F-00 013) 5 megapixel interpolated webcam with a resolution of 1920×1080 pixels, which was placed 30 cm above the sample tray to capture images during the drying process. The lighting system consists of LED lamps mounted at a 45-degree angle above the sample tray to ensure uniform illumination. The processing unit controls the camera settings via a developed graphical user interface (GUI) and allows images to be captured and stored in real time. The images

were captured every 300 seconds and stored in JPEG format (544×960 resolution, RGB 24-bit color space) for further analysis. A schematic representation of the experimental setup can be found in Figure 1, which visually illustrates the equipment and workflow. In the following sections, the drying process and the developed machine vision system are explained in detail.

Sample preparation and drying

In this paper, the drying process of Shahani variety of date fruits is studied. To this end, several palm trees from Jahrom city in Fars province of Iran were randomly chosen for the sampling of date fruits at the stage of Kharak (with an initial moisture content of 60 % d.b.). The collected samples were kept in nylon packs and refrigerated at 9 °C before the drying process (Martynenko & Zheng, 2016).

To prepare the samples for drying, they were kept at room temperature for about three hours outside the refrigerator. Then, the date fruits were cut into 3 mm thin slices using a Bora Electric (Model 250, Iran) slicer. Each drying experiment based on Table 1 was conducted with 9 slices date fruits of an approximate total weight of 10 grams at three different temperatures (i.e., 25, 30, and 60 °C), and three different levels of air velocity (0.5, 1.0, and 1.5 m/s) (Keramat-Jahromi *et al.*, 2021).

Table 1. Experiments and operational parameters for drying process

Experiment No.	1	2	3	4	5	6	7	8	9
Temperature (°C)	25	25	25	30	30	30	60	60	60
Air velocity (m/s)	0.5	1	1.5	0.5	1	1.5	0.5	1	1.5
EHD (W)	1	1	1	1	1	1	1	1	1

The EHD dryer consists of 16 needle electrodes 40 mm long with a square arrangement of 30 mm apart. The thin layers of dates were placed between the needle electrodes so that they could be imaged from the top of the drying chamber. The distance between the end of the needle electrodes and the ground plate electrodes was 3 cm. Ground plate electrodes were also made of copper plate 18 × 18 cm². The power level of the device was set to 1.0W of a high-voltage source (Model D-RC Series, FanavaranNano-Meghyas,

Iran), and the experiments were conducted in a full factorial design at room temperature of 25 °C. Each experiment was repeated three times and the drying was carried on to reduce the moisture ratio (MR) of the fruits to 0.2 (Keramat-Jahromi *et al.*, 2021).

The Imaging Unit

During the drying process, images of the samples were captured at regular time intervals and processed in real-time. The captured images

were saved in an RGB color format and later converted to the Lab* color space for better color representation. A background removal technique was applied to isolate the sample from the background, ensuring accurate feature extraction. The extracted color and texture features were then used as inputs for the Adaptive Neuro-Fuzzy Inference System (ANFIS) model to predict the moisture ratio (MR). The overall image acquisition and processing workflow is illustrated in Figure 1, providing a schematic representation of the methodology used in this study.

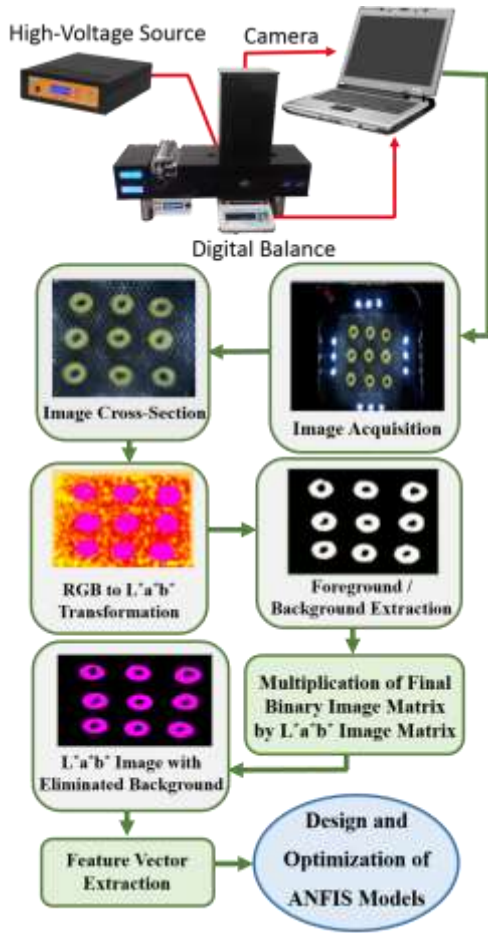


Figure 1. The general scheme of the research and data collection

The processing unit

The processing unit exploited algorithms developed in MATLAB to simultaneously

process the captured images. Initially, the obtained RGB color values were calibrated using a 24-color chart x-rite color checker. Next, to extract discriminative features from the captured images for analysing the moisture level of the dried date fruits, RGB images were transformed into L*a*b* color space. The L*a*b* is a very popular color space in the food industry due to its uniform distribution of colors and its similarity to human perception of colors. Then, Otsu thresholding was used to remove the background of the images. After eliminating the background of the images, four different sets of features were extracted based on Table 2. These extracted features were then introduced into an ANFIS model to estimate the MR of the date fruits. Adaptive neuro fuzzy inference system (ANFIS) has been used by numerous studies (Miraei Ashtiani *et al.*, 2020; Okonkwo *et al.*, 2022). The extracted features and the developed ANFIS model are described further. The performance of the developed model with a different set of features as input is analysed and compared in the next section.

Table 2. Extracted features as different entrance sets of ANFIS model to estimate MR

Set No.	Extracted features
1	Temperature (T), air velocity (V), time (t)
2	T, V, time, $\bar{L}^*(t)$, $\bar{a}^*(t)$, and $\bar{b}^*(t)$
3	T, V, time, $\bar{L}^*(t)$, $\bar{a}^*(t)$, $\bar{b}^*(t)$, $\bar{L}^*(t)$, $\bar{a}^*(t)$, $\bar{b}^*(t)$, $\bar{L}^*(t-1)$, $\bar{a}^*(t-1)$, and $\bar{b}^*(t-1)$
4	T, V, time, $\bar{L}^*(t)$, $\bar{a}^*(t)$, $\bar{b}^*(t)$, $\bar{L}^*(t)$, $\bar{a}^*(t)$, $\bar{b}^*(t)$, $\bar{L}^*(t-1)$, $\bar{a}^*(t-1)$, $\bar{b}^*(t-1)$, $\bar{L}^*(t-2)$, $\bar{a}^*(t-2)$, and $\bar{b}^*(t-2)$

ANFIS, known as the adaptive neuro-fuzzy inference system, is an effective combination of artificial neural networks (ANN) and fuzzy logic. In the ANFIS model, the fuzzy inference system (FIS) is combined with the trainable characteristics of ANN to generate a trainable model with the generalization capability of fuzzy logic. ANFIS is structured as five layers, i.e., input fuzzification, fuzzy set database construction, fuzzy rule base construction, decision-making, and output defuzzification. The fuzzification process is performed through passing input data from membership functions. Then, a set of if-then rules is applied to obtain the output characteristics. The output defuzzification stage is performed using the output membership functions to reach a single-valued output or a decision associated with the output. The hybrid learning algorithm, which is a combination of back-propagation gradient descent and the least-squares method, was used for training parameters of the fuzzy inference system (Miraei Ashtiani *et al.*, 2020). Four different ANFIS models corresponding to four different feature sets were trained to predict the MR of the dried date fruits. Each of the developed ANFIS models was designed with six deferent membership functions, including the Gaussin (Gaussmf), bell (gbellmf), sigmoid (sigmf), differential sigmoid (dsig), multiply sigmoid (psig), and the S shape (smf) function, and the results were compared to choose the best model.

Evaluating performance

The performance of the models is evaluated using five criteria, including the root mean square error (*RMSE*), mean absolute error (*MAE*), relative absolute error (*RAE*), coefficient of

determination (r^2), and conformity index (d), which are defined as follows (equations 2-1 to 2-5, respectively):

$$RMSE = \sqrt{\frac{\sum_{i=1}^n (y_i - \hat{y}_i)^2}{n}} \quad (1)$$

$$MAE = \frac{\sum_{i=1}^n |y_i - \hat{y}_i|}{n} \quad (2)$$

$$RAE = \frac{\sum_{i=1}^n |y_i - \hat{y}_i|}{\sum_{i=1}^n |y_i - \bar{y}|} \quad (3)$$

$$r^2 = \left(\frac{\sum_{i=1}^n (y_i - \bar{y})(\hat{y}_i - \bar{\hat{y}})}{\sqrt{\sum_{i=1}^n (y_i - \bar{y})^2} \sqrt{\sum_{i=1}^n (\hat{y}_i - \bar{\hat{y}})^2}} \right)^2 \quad (4)$$

$$d = 1 - \frac{\sum_{i=1}^n (y_i - \hat{y}_i)^2}{\sum_{i=1}^n (|\hat{y}_i - \bar{\hat{y}}| + |y_i - \bar{y}|)^2} \quad (5)$$

In these equations, n is the total number of data, y_i denotes the real observed value of the MR of the i 'th data, \hat{y}_i shows the model's predicted value of the MR, and \bar{y} and $\bar{\hat{y}}$ represent the mean values of the observed and predicted MR, respectively.

RESULTS AND DISCUSSION

In this section, the designed ANFIS models with different feature sets and different membership functions are tested and compared for estimating the MR of the dried date fruits. The prediction results of the MR for the four different sets of ANFIS inputs for training and test data are presented in Tables 3 and 4, respectively. Note that these results are relevant to the entire data set and are not limited to the specific speed and temperature of the experiment. The selection of the best ANFIS model was based on several evaluation measures, including the coefficient of determination (r^2), root mean square error (*RMSE*), mean absolute error (*MAE*) and relative

absolute error (RAE). While some models achieved higher R^2 values and lower RMSE, we considered the generalization performance on the test data as a key factor for selecting the optimal model.

In particular, models showing high R^2 values (0.99) and low RMSE during training, but suboptimal R^2 and RMSE during testing, displayed overfitting, resulting in a significant performance gap. To obtain a more generalizable and reliable model, we chose the ANFIS model with six inputs and the differential sigmoid (dsig)

membership function, which provides a good balance between accuracy and robustness. This model had an r^2 of 0.988 for the training data and 0.987 for the test data, along with a competitive RMSE of 0.025, ensuring stable performance under different experimental conditions. Comparison of the performance of models with three and six inputs indicates that the use of visual properties improves the estimation of the MR. In the ANFIS model with nine inputs, the differential sigmoid membership function again had the best performance.

Table 3. Statistical indices of ANFIS model for predicting MR (training data)

Model No.	Number of entries	Membership function	d	RAE	RMSE	MAE	R^2
1	3	gaussmf	0.99997	0.080	0.042	0.015	0.966
2	3	gbellmf	0.99996	0.014	0.052	0.027	0.947
3	3	Dsigmf	0.99997	0.077	0.041	0.015	0.967
4	3	Psigmf	0.99997	0.108	0.045	0.021	0.961
5	3	Sigmf	0.99996	0.123	0.048	0.024	0.956
6	3	Smf	0.99997	0.108	0.045	0.021	0.961
7	6	gaussmf	0.99998	0.083	0.039	0.016	0.970
8	6	gbellmf	0.99997	0.119	0.045	0.023	0.962
9	6	dsigmf	0.99999	0.076	0.025	0.015	0.988
10	6	Psigmf	0.99997	0.101	0.042	0.020	0.966
11	6	Sigmf	0.99998	0.107	0.039	0.021	0.971
12	6	Smf	0.99997	0.101	0.042	0.020	0.967
13	9	gaussmf	0.99997	0.090	0.035	0.015	0.971
14	9	gbellmf	0.99996	0.144	0.044	0.025	0.954
15	9	Dsigmf	0.99999	0.083	0.025	0.014	0.985
16	9	Psigmf	0.99997	0.112	0.040	0.019	0.961
17	9	Sigmf	0.99998	0.116	0.034	0.020	0.973
18	9	Smf	0.99998	0.079	0.027	0.014	0.983
19	12	gaussmf	0.99997	0.109	0.034	0.017	0.965
20	12	gbellmf	0.99996	0.152	0.038	0.024	0.957
21	12	Dsigmf	0.99999	0.084	0.018	0.013	0.990
22	12	Psigmf	0.99997	0.110	0.034	0.017	0.965
23	12	Sigmf	0.99997	0.104	0.030	0.016	0.973
24	12	Smf	0.99998	0.075	0.024	0.012	0.983

According to the results, the ANFIS model with nine inputs was not as efficient as the model with six inputs. While increasing the number of inputs initially improved prediction accuracy, further increasing the number of inputs beyond six resulted in diminishing returns and potential overfitting. Although the differential sigmoid

membership function in the 12-input ANFIS model showed the best performance during training ($R^2=0.99$), it was not selected as the best model due to its poor generalization in the testing phase ($R^2=0.927$), indicating overfitting to the training data.

Figure 2 further illustrates this effect by

showing how the number of inputs affects the model's performance on the test data. Figure 2(a) shows that R^2 increases from 3 to 6 inputs and reaches a peak value, but decreases as more inputs are added. Similarly, Figure 2(b) shows that the RMSE decreases significantly from 3 to 6 inputs, indicating a better fit. However, for more than six inputs, the RMSE increases, indicating that adding too many inputs leads to noise instead of improving the predictive power. Figure 3 and Figure 4 display the distribution of estimated values and actual data by the differential sigmoidal function (dsig) in the six-input ANFIS model for the training and test data, respectively.

Figure 5 reveals a graph of the estimation of MR based on air velocity and time of experiment.

Figure 6 presents the estimation of MR based on the experiment temperature and time, where the maximum MR is yellow and the minimum is blue. As seen in Figure 5, the final MR was set to 0.2, which occurred at the maximum time, the end of the drying process, which is consistent with the test evidence. The corresponding airflow velocity corresponding to this minimum is estimated to be 0.5 m/s. The maximum MR was estimated at zero at the beginning of the process at 1.5 m/s. According to Figure 6, the lowest MR has occurred at the maximum time and minimum temperatures. These values are perfectly consistent since the MR is inversely correlated with time and temperature while being directly related to the airflow rate.

Table 4. Statistical indices of ANFIS model for predicting MR (test data)

Model No.	Number of entries	Membership function	d	RAE	RMSE	MAE	R^2
1	3	gaussmf	0.99994	0.074	0.040	0.014	0.970
2	3	Gbellmf	0.99991	0.013	0.050	0.027	0.955
3	3	Dsigmf	0.99994	0.065	0.041	0.013	0.970
4	3	Psigmf	0.99993	0.102	0.043	0.020	0.966
5	3	Sigmf	0.99993	0.117	0.044	0.023	0.966
6	3	Smf	0.99993	0.109	0.043	0.021	0.967
7	6	gaussmf	0.99993	0.088	0.043	0.017	0.963
8	6	Gbellmf	0.99991	0.123	0.049	0.023	0.954
9	6	Dsigmf	0.99998	0.086	0.025	0.016	0.987
10	6	Psigmf	0.99991	0.102	0.047	0.020	0.956
11	6	Sigmf	0.99991	0.114	0.050	0.022	0.951
12	6	Smf	0.99991	0.109	0.048	0.021	0.955
13	9	gaussmf	0.99983	0.171	0.059	0.029	0.918
14	9	Gbellmf	0.99989	0.175	0.046	0.030	0.949
15	9	Dsigmf	0.99993	0.117	0.038	0.020	0.964
16	9	Psigmf	0.99991	0.143	0.043	0.024	0.954
17	9	Sigmf	0.9999	0.169	0.045	0.029	0.949
18	9	Smf	0.99991	0.115	0.041	0.020	0.959
19	12	gaussmf	0.99983	0.195	0.049	0.029	0.927
20	12	Gbellmf	0.99961	0.263	0.073	0.039	0.939
21	12	Dsigmf	0.99983	0.162	0.049	0.024	0.927
22	12	Psigmf	0.99982	0.171	0.049	0.026	0.924
23	12	Sigmf	0.99986	0.153	0.043	0.023	0.941
24	12	Smf	0.99986	0.143	0.044	0.021	0.939

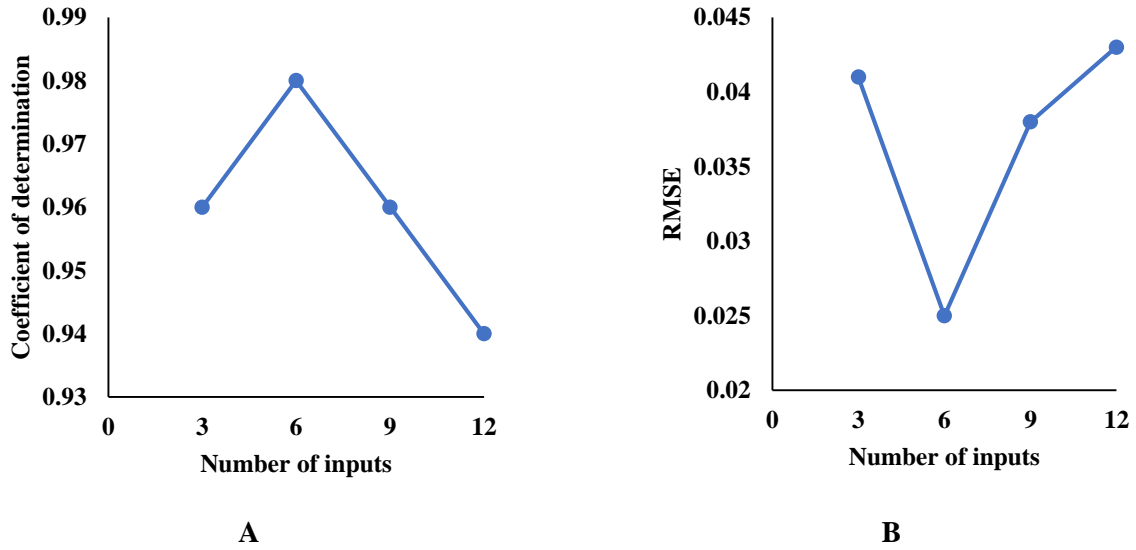


Figure 2. Effect of the number of input features on model performance for test data: (a) Coefficient of determination (R^2), and (b) Root Mean Square Error (RMSE).

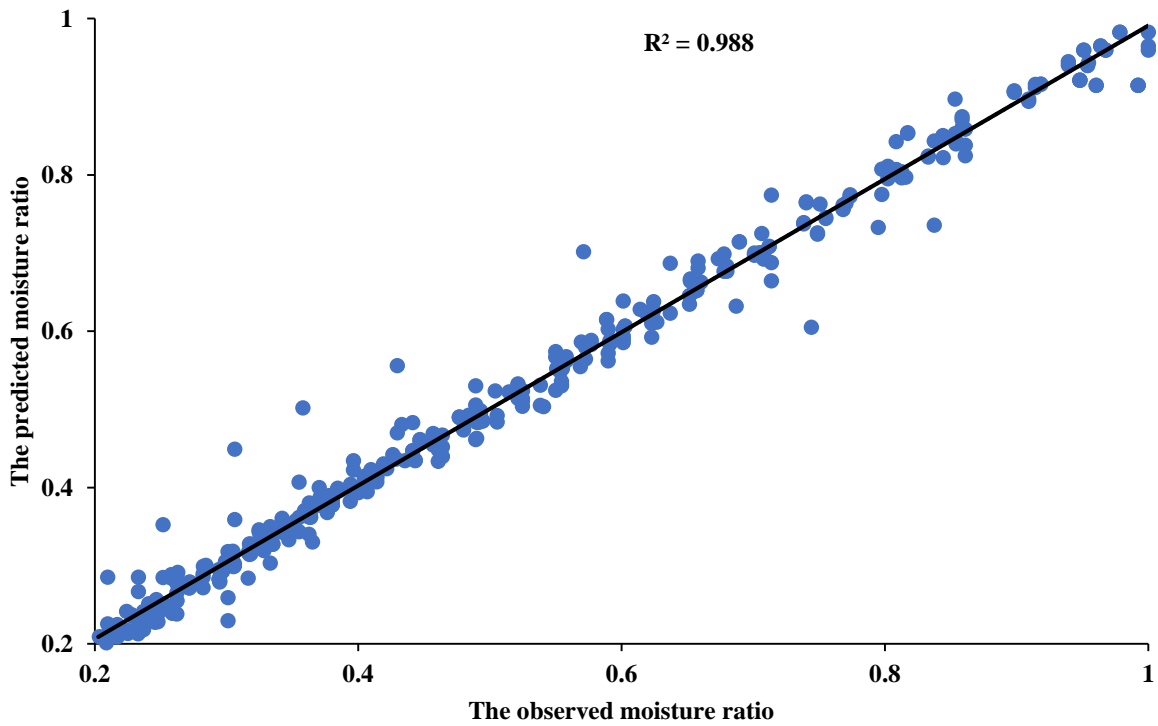


Figure 3. The relationship between the observed and predicted MR using AFNIS model (training data)

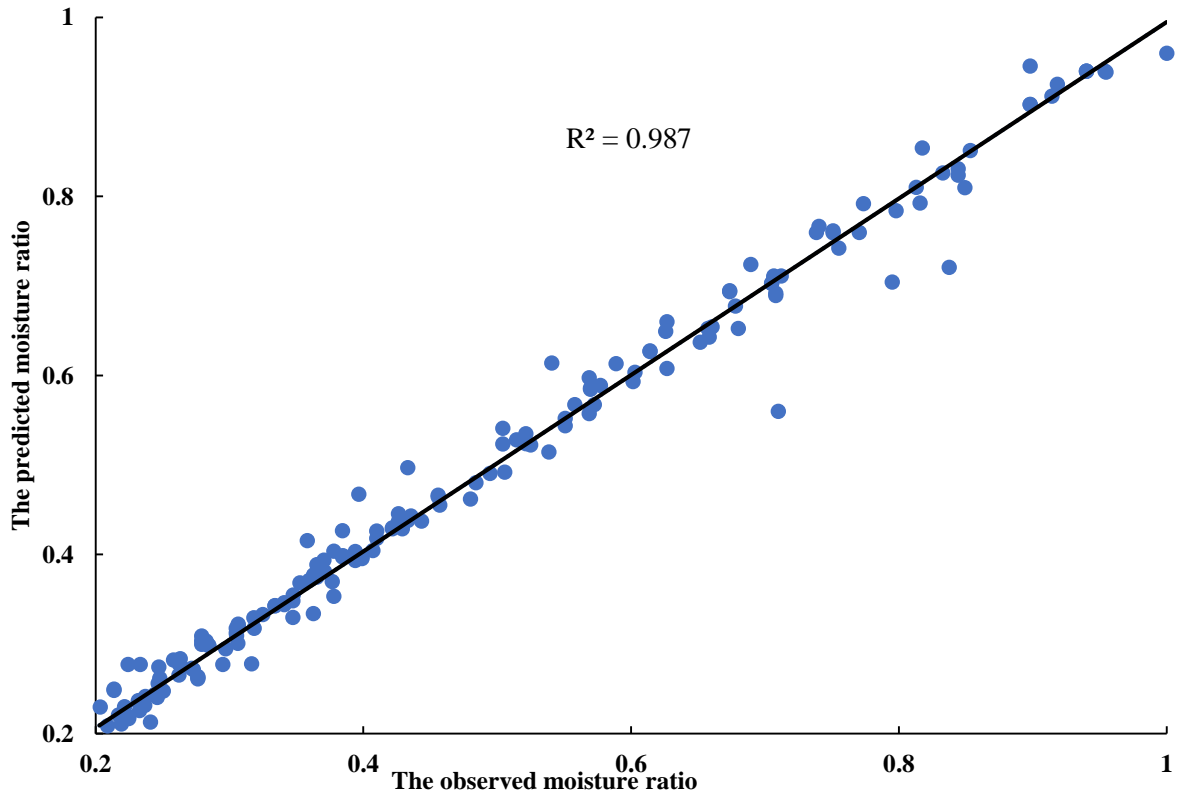


Figure 4. The relationship between the observed and predicted MR using AFNIS model (test data)

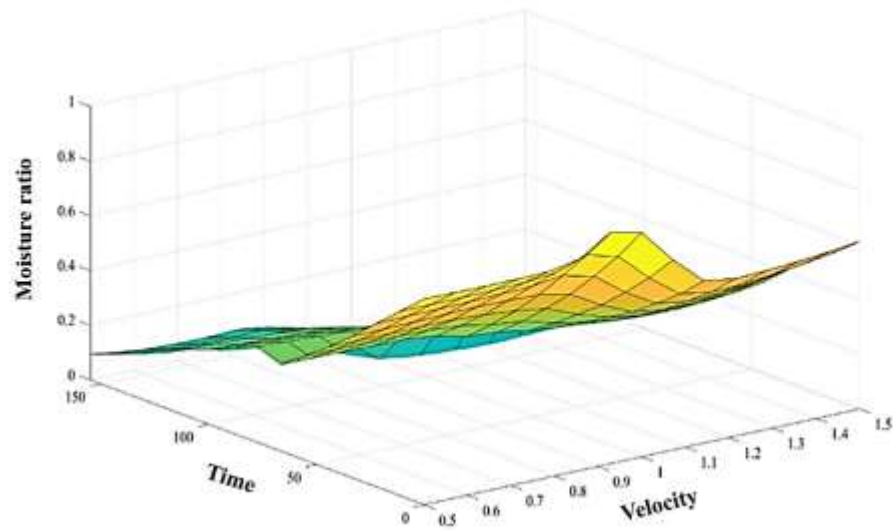


Figure 5. Modeling of MR based on interaction of air velocity and drying time

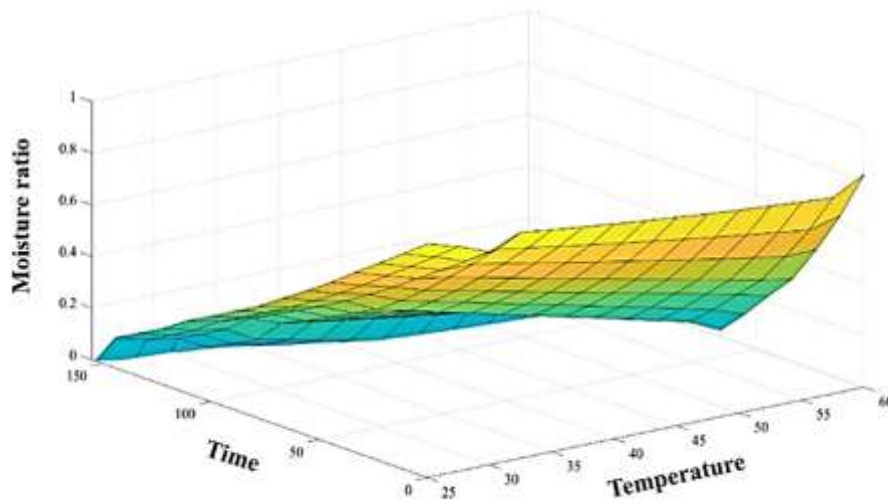


Figure 6. Modeling of MR based on interaction of temperature of chamber and drying time

Figure 7 depicts the other graphs of the estimated MR values in the ANFIS model by a six-input differential sigmoidal function based on physical properties and an image property. As expected in this graph, the blue or minimum response points are modelled at higher times and

temperatures. According to Figure7 (e), in the graph of the estimation of the MR based on temperature and a^* , the maximum response variable at low temperature is predicted, while for higher values of a^* it has a relatively higher value.

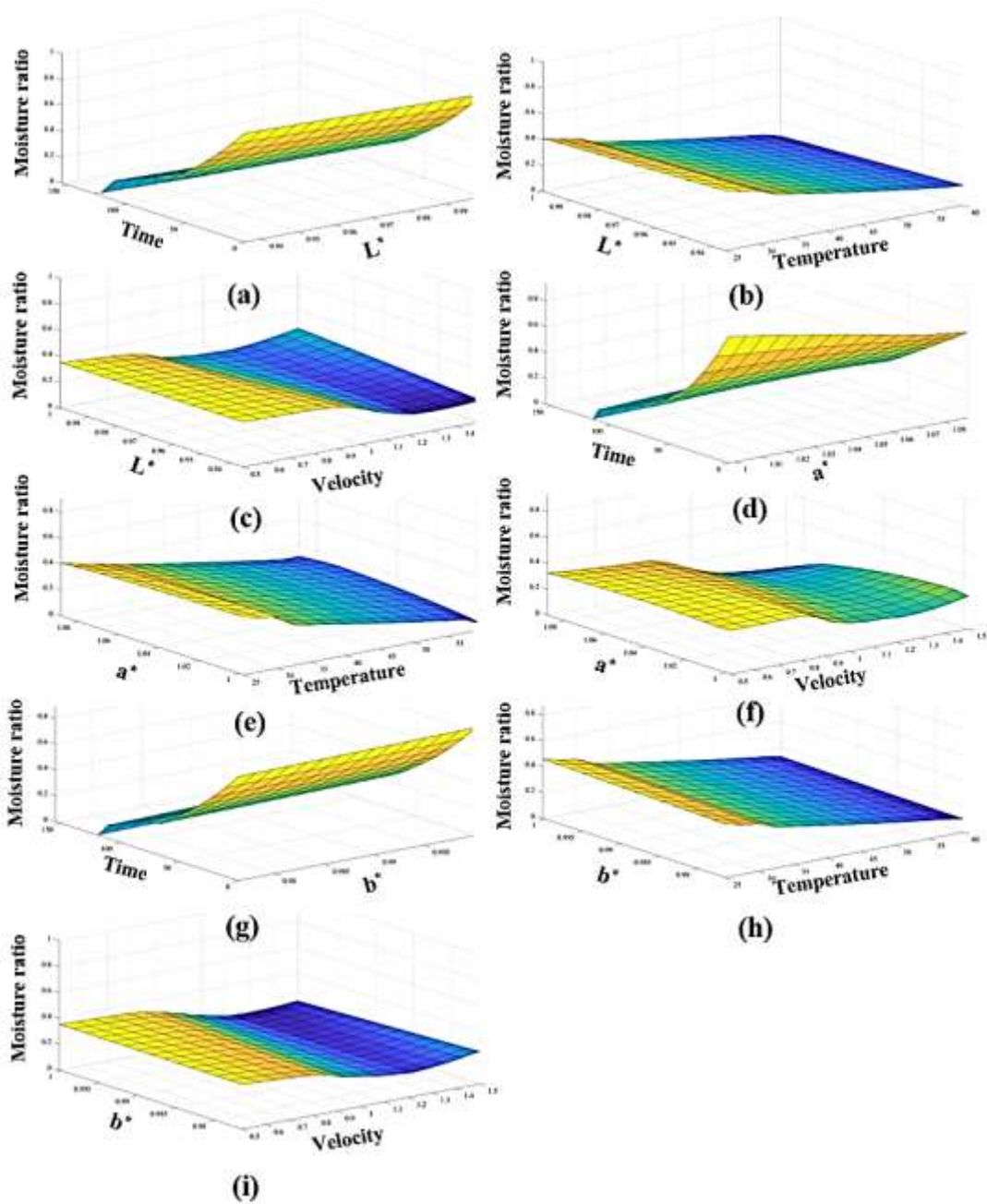


Figure 7. Estimation of MR based on interaction of (a) L^* and drying time, (b) temperature of chamber and L^* , (c) air velocity and L^* , (d) a^* and drying time, (e) temperature of chamber and a^* , (f) air velocity and a^* , (g) b^* and drying time, (h) temperature of chamber and b^* , and (i) air velocity and b^*

In order to evaluate the quality of developed model, several experimental and regression models were developed and compared with the ANFIS model to estimate the MR. Models 1-6 are

experimental models. The best experimental model for prediction of MR is model 5, which has had a lower performance ($R^2=0.755$) than ANFIS model (Table 5).

Table 5. Statistical indicators of experimental and regression models for prediction of MR (test data)

Model No.	Form	Coefficients	d	RAE	RMSE	MAE	R ²
1	$a \exp(-kt) + b \exp(-gt)$	$a = -0.499\ 6; k = 0.051\ 5;$ $b = -0.469\ 3; g = 0.004\ 8$	0.926	0.46	0.114	0.092	0.753
2	$a \exp(-kt) + c$	$a = 0.678\ 6; k = 0.034\ 6;$ $c = 0.274\ 7$	0.924	0.47	0.115	0.094	0.748
3	$1 + at + bt^2$	$a = -0.016\ 5; b = 0.000\ 1$	0.907	0.56	0.140	0.112	0.686
4	$a \exp(-kt) + (1 - a) \exp(-gt)$	$a = 0.497; b = 0.005\ 4;$ $g = 0.058\ 9$	0.928	0.47	0.114	0.092	0.754
5	$a \exp(-kt) + b \exp(-gt) + c \exp(-ht)$	$a = 2.638; b = -0.533\ 9;$ $c = -2.218; k = 0.098\ 1;$ $g = 0.006; h = 0.110\ 7;$	0.926	0.46	0.114	0.092	0.755
6	$a \exp(-kt) + \exp(-gt)$	$a = -0.042\ 9; k = 5.252;$ $g = 0.017\ 5$ $a_0 = 1.244\ 8; a_1 = -0.008$	0.91	0.60	0.144	0.118	0.702
7	$a_0 + a_1 T + a_2 V + a_3 t$	$a_2 = -0.112\ 8; a_3 = -0.006\ 4$ $a_0 = 6.488\ 8; a_1 = -0.005\ 6;$	0.944	0.38	0.101	0.076	0.806
8	$a_0 + a_1 T + a_2 V + a_3 t + a_4 \bar{L}^* + a_5 \bar{a}^* + a_6 \bar{b}^*$	$a_2 = -0.109; a_3 = -0.005;$ $a_4 = 1.872\ 3; a_5 = -2.706\ 6;$ $a_6 = -4.482\ 2$	0.957	0.35	0.090	0.069	0.847
9	$a_0 + a_1 T + a_2 V + a_3 t + a_4 Tt$	$a_0 = 1.045\ 5; a_1 = -0.002\ 1;$ $a_2 = -0.120\ 6; a_3 = 0.000\ 1;$ $a_4 = -0.000\ 2$	0.973	0.29	0.073	0.058	0.899
10	$a_0 + a_1 T + a_2 V + a_3 t + a_4 Vt$	$a_0 = 1.134\ 7; a_1 = -0.008\ 4;$ $a_2 = 0.022\ 3; a_3 = -0.004\ 1;$ $a_4 = -0.002\ 8$	0.954	0.35	0.092	0.069	0.838
11	$a_0 + a_1 T + a_2 V + a_3 t + a_4 Tt + a_5 Vt$	$a_0 = 0.964\ 4; a_1 = -0.002\ 6;$ $a_2 = -0.008\ 1; a_3 = 0.001\ 7;$ $a_4 = -0.000\ 2; a_5 = -0.002\ 3$	0.979	0.26	0.064	0.051	0.921

The results of regression models in Table 5 (models 7-12) indicate that model 11 has had the highest modelling performance ($R^2=0.921$), which is still lower than ANFIS accuracy. Then, we conclude that the ANFIS model has outperformed the other models in predicting the MR.

CONCLUSIONS

The results of this study show that the inclusion of visual features in the ANFIS model significantly improves the accuracy of MR estimation during the drying process. In particular, the ANFIS model with six inputs and the differential sigmoid (dsig) membership function provided the best prediction performance with coefficients of determination

(R^2) of 0.988 for training data and 0.987 for test data. Increasing the number of inputs to nine and twelve initially improved training performance but resulted in lower generalization ability in the test phase, with the twelve-input model outperforming the training data ($R^2=0.99$) but not generalizing well ($R^2=0.927$). These results confirm that a balance between input complexity and model generalization is essential for robust MR prediction. Furthermore, the study highlights the potential of machine vision systems for real-time monitoring of drying processes in EHD convection dryers. The developed ANFIS-based model offers a reliable alternative to conventional weighing systems, which are prone to noise interference. The ability to use image-based analysis for real-time quality control is an

important step towards intelligent and automated drying processes in the food industry.

Acknowledgments

This study was funded by Iran National Science Foundation (INSF) with project number 96000212. The authors would like to acknowledge the valuable comments and suggestions of Dr. Ehsan Savand-Roumi which have improved the quality of this paper.

REFERENCES

- Aghbashlo, M., Hosseinpour, S., & Ghasemi-Varnamkhasti, M. (2014). Computer vision technology for real-time food quality assurance during drying process. *Trends in Food Science and Technology*, 39(1), 76–84. <https://doi.org/10.1016/j.tifs.2014.06.003>
- Aghilinategh, N., Rafiee, S., Hosseinpour, S., Omid, M., & Mohtasebi, S. S. (2016). Real-time color change monitoring of apple slices using image processing during intermittent microwave convective drying. *Food Science and Technology International*, 22(7), 634–646. <https://doi.org/10.1177/1082013216636263>
- Anukiruthika, T., Moses, J. A., & Anandharamkrishnan, C. (2021). Electrohydrodynamic drying of foods: Principle, applications, and prospects. *Journal of Food Engineering*, 295, 110449. <https://doi.org/10.1016/j.jfoodeng.2020.110449>
- Bashkir, I., Defraeye, T., Kudra, T., & Martynenko, A. (2020). Electrohydrodynamic Drying of Plant-Based Foods and Food Model Systems. *Food Engineering Reviews*, 12(4), 473–497. <https://doi.org/10.1007/s12393-020-09229-w>
- Benalia, S., Cubero, S., Prats-Montalbán, J. M., Bernardi, B., Zimbalatti, G., & Blasco, J. (2016). Computer vision for automatic quality inspection of dried figs (*Ficus carica* L.) in real-time. *Computers and Electronics in Agriculture*, 120, 17–25. <https://doi.org/10.1016/j.compag.2015.11.002>
- Bora, G. C., Pathak, R., Ahmadi, M., & Mistry, P. (2018). Image processing analysis to track colour changes on apple and correlate to moisture content in drying stages. *Food Quality and Safety*, 2(2), 105–110. <https://doi.org/10.1093/fqsafe/fyy003>
- Esehaghbeygi, A., Pirnazari, K., & Sadeghi, M. (2014). Quality assessment of electrohydrodynamic and microwave dehydrated banana slices. *Lwt -Food Science and Technology*, 55(2), 565–571. <https://doi.org/10.1016/j.lwt.2013.10.010>
- Gao, K., Zhou, L., Bi, J., Yi, J., Wu, X., Zhou, M., Wang, X., & Liu, X. (2017). Evaluation of browning ratio in an image analysis of apple slices at different stages of instant controlled pressure drop-assisted hot-air drying (AD-DIC). *Journal of the Science of Food and Agriculture*, 97(8), 2533–2540. <https://doi.org/10.1002/jsfa.8070>
- Ghaitaranpour, A., Rastegar, A., Tabatabaei Yazdi, F., Mohebbi, M., & Alizadeh Behbahani, B. (2017). Application of Digital Image Processing in Monitoring some Physical Properties of Tarkhineh during Drying. *Journal of Food Processing and Preservation*, 41(2), e12861. <https://doi.org/10.1111/jfpp.12861>
- Hosseinpour, S., Rafiee, S., Aghbashlo, M., & Mohtasebi, S. S. (2015). Computer Vision System (CVS) for In-Line Monitoring of Visual Texture Kinetics During Shrimp (*Penaeus* Spp.) Drying. *Drying Technology*, 33(2), 238–254. <https://doi.org/10.1080/07373937.2014.947513>
- Hosseinpour, S., Rafiee, S., Mohtasebi, S. S., & Aghbashlo, M. (2013). Application of computer vision technique for on-line monitoring of shrimp color changes during drying. *Journal of Food Engineering*, 115(1), 99–114. <https://doi.org/10.1016/j.jfoodeng.2012.10.003>
- Iranshahi, K., Onwude, D. I., Martynenko, A., & Defraeye, T. (2022). Dehydration mechanisms in electrohydrodynamic drying of plant-based foods. *Food and Bioproducts Processing*, 131, 202–216. <https://doi.org/10.1016/j.fbp.2021.11.009>
- Keramat-Jahromi, M., Mohtasebi, S. S., Mousazadeh, H., Ghasemi-Varnamkhasti, M., & Rahimi-Movassagh, M. (2021). Real-time moisture ratio study of drying date fruit chips based on on-line image attributes using kNN and random forest regression methods. *Measurement*, 172, 108899. <https://doi.org/10.1016/j.measurement.2020.108899>
- Kırbaç, İ., Tuncer, A. D., Şirin, C., & Usta, H. (2019). Modeling and developing a smart interface for various drying methods of pomelo fruit (*Citrus maxima*) peel using machine learning approaches. *Computers and Electronics in Agriculture*, 165, 104928.

- <https://doi.org/10.1016/j.compag.2019.104928>
- Martynenko, A. (2017).** Computer Vision for Real-Time Control in Drying. *Food Engineering Reviews*, 9, 91–111. <https://doi.org/10.1007/s12393-017-9159-5>
- Martynenko, A., Astatkie, T., Riaud, N., Wells, P., & Kudra, T. (2017).** Driving forces for mass transfer in electrohydrodynamic (EHD) drying. *Innovative Food Science and Emerging Technologies*, 43, 18–25. <https://doi.org/10.1016/j.ifset.2017.07.022>
- Martynenko, A., & Kudra, T. (2016).** Electrically-induced transport phenomena in EHD drying - A review. *Trends in Food Science and Technology*, 54, 63–73. <https://doi.org/10.1016/j.tifs.2016.05.019>
- Martynenko, A., & Zheng, W. (2016).** Electrohydrodynamic drying of apple slices: Energy and quality aspects. *Journal of Food Engineering*, 168, 215–222. <https://doi.org/10.1016/j.jfoodeng.2015.07.043>
- Miraei Ashtiani, S. H., Rohani, A., & Aghkhani, M. H. (2020).** Soft computing-based method for estimation of almond kernel mass from its shell features. *Scientia Horticulturae*, 262, 109071. <https://doi.org/10.1016/j.scienta.2019.109071>
- Miraei Ashtiani, S. H., Sturm, B., & Nasirahmadi, A. (2018).** Effects of hot-air and hybrid hot air-microwave drying on drying kinetics and textural quality of nectarine slices. *Heat and Mass Transfer*, 54, 915–927. <https://doi.org/10.1007/s00231-017-2187-0>
- Mirzaei-Baktash, H., Hamdami, N., Torabi, P., Fallah-Joshaqani, S., & Dalvi-Isfahan, M. (2022).** Impact of different pretreatments on drying kinetics and quality of button mushroom slices dried by hot-air or electrohydrodynamic drying. *Lwt*, 155, 112894. <https://doi.org/10.1016/j.lwt.2021.112894>
- Nadian, M. H., Abbaspour-Fard, M. H., Sadriani, H., Golzarian, M. R., Tabasizadeh, M., & Martynenko, A. (2017).** Improvement of kiwifruit drying using computer vision system (CVS) and ALM clustering method. *Drying Technology*, 35(6), 709–723. <https://doi.org/10.1080/07373937.2016.1208665>
- Nadian, M. H., Rafiee, S., Aghbashlo, M., Hosseinpour, S., & Mohtasebi, S. S. (2015).** Continuous real-time monitoring and neural network modeling of apple slices color changes during hot air drying. *Food and Bioprocess Processing*, 94, 263–274. <https://doi.org/10.1016/j.fbp.2014.03.005>
- Okonkwo, C. E., Olaniran, A. F., Adeyi, A. J., Adeyi, O., Ojediran, J. O., Erinle, O. C., Mary, I. Y., & Taiwo, A. E. (2022).** Neural network and adaptive neuro-fuzzy inference system modeling of the hot air-drying process of orange-fleshed sweet potato. *Journal of Food Processing and Preservation*, 46(3), e16312. <https://doi.org/10.1111/jfpp.16312>
- Paul, A., & Martynenko, A. (2021).** Electrohydrodynamic drying: Effects on food quality. *Drying Technology*, 39(11), 1745–1761. <https://doi.org/10.1080/07373937.2021.1906694>
- Pirnazari, K., Esehaghbeygi, A., & Sadeghi, M. (2014).** Assessment of quality attributes of banana slices dried by different drying methods. *International Journal of Food Engineering*, 10(2), 251–260. <https://doi.org/10.1515/ijfe-2013-0059>
- Polat, A., & Izli, N. (2022a).** Drying characteristics and quality evaluation of ‘Ankara’ pear dried by electrohydrodynamic-hot air (EHD) method. *Food Control*, 134, 108774. <https://doi.org/10.1016/j.foodcont.2021.108774>
- Polat, A., & Izli, N. (2022b).** Drying of garlic slices by electrohydrodynamic-hot air method. *Journal of Food Process Engineering*, 45(3), e13980. <https://doi.org/10.1111/jfpe.13980>
- Pu, Y. Y., & Sun, D. W. (2017).** Combined hot-air and microwave-vacuum drying for improving drying uniformity of mango slices based on hyperspectral imaging visualisation of moisture content distribution. *Biosystems Engineering*, 156, 108–119. <https://doi.org/10.1016/j.biosystemseng.2017.01.006>
- Raj, G. V. S. B., & Dash, K. K. (2020).** Microwave vacuum drying of dragon fruit slice: Artificial neural network modelling, genetic algorithm optimization, and kinetics study. *Computers and Electronics in Agriculture*, 178, 105814. <https://doi.org/10.1016/j.compag.2020.105814>
- Shafaei, S. M., Nourmohamadi-Moghadami, A., & Kamgar, S. (2016).** Development of artificial intelligence based systems for prediction of hydration characteristics of wheat. *Computers and Electronics in Agriculture*, 128, 34–45. <https://doi.org/10.1016/j.compag.2016.08.014>
- Taghian Dinani, S., Hamdami, N., Shahedi, M., &**

Havet, M. (2014). Mathematical modeling of hot air/electrohydrodynamic (EHD) drying kinetics of mushroom slices. *Energy Conversion and Management*, 86, 70–80. <https://doi.org/10.1016/j.enconman.2014.05.010>

Udomkun, P., Nagle, M., Argyropoulos, D., Wiredu, A. N., Mahayothee, B., & Müller, J. (2017). Computer vision coupled with laser backscattering for non-destructive colour evaluation of papaya during drying. *Journal of Food Measurement and Characterization*, 11, 2142–2150. <https://doi.org/10.1007/s11694-017-9598-y>